Atmosphere-cryosphere interactions during the last phase of the LGM (21 ka BP) in the European Alps

Costanza Del Gobbo[1, 2], Renato R. Colucci[1, 3], Giovanni Monegato[4], Manja Žebre[5], Filippo Giorgi[2]

[1] Institute of Polar Sciences, National Research Council, Trieste, 34149, Italy
[2] Abdus Salam International Centre for Theoretical Physics, Trieste, 34151, Italy
[3] Alpine-Adriatic Meteorological Society, Udine, 33100, Italy
[4] Institute of Geosciences and Earth Resources, National Research Council, Padova, 35131, Italy
[5] Geological Survey of Slovenia, Ljubljana, 1000, Slovenia

Correspondence to: Costanza Del Gobbo (costanza.delgobbo@gmail.com)

Abstract. Evidence that during the Last Glacial Maximum (LGM) glaciers extended well into the piedmont planes is still identifiable in the alpine foreland as a system of well-preserved moraines. Glaciers are strongly controlled by temperature and precipitation and therefore they are excellent indicators of climate change. Here we use a regional climate model (RCM) to investigate some of the physical processes sustaining Alpine glaciers during the last phase of the LGM, at 21 ka BP. We find a predominance of convection during summer and increased southwesterly stratiform precipitation over the southern Alps compared to pre-industrial (PI) conditions. This precipitation pattern, along with lower temperatures, determined summer snowfall extending to low elevations with a consequent substantial drop of the equilibrium line altitude (ELA) consistent with the estimated LGM glacier extent. Our RCM based estimates of the 21 ka BP ELA at the LGM yield excellent consistency with Alpine ELA reconstructions, further demonstrating the great potential of this technique for use in paleoclimate studies.

1 Introduction

The Last Glacial Maximum (LGM) was a period of maximum global ice volume (Hughes et al., 2013) during the last glacial cycle (0 to 150 ka BP; Lisiecki and Stern, 2016), and it extended approximately from 26.5 to 19 ka BP (Clark et al., 2009). It is conventionally defined by a minimum in global sea-level (Peltier and Fairbanks, 2006; Lambeck et al., 2014) and a maximum in marine oxygen isotope records (Mix et al., 2001). However, although the LGM is considered to be a global event, there is evidence (Hughes et al., 2013; Clark et al., 2009; Monegato et al., 2017) that it did not occur synchronously worldwide, with mountain glaciers and ice sheets reaching their maximum extent at different times and being out-of-phase with respect to the signal of marine isotope records (Hughes et al., 2013).

The European Alps have been widely affected by the LGM glacier advance. The Alps' interconnected valley glaciers, icefields (Kelly et al., 2004; Ivy-Ochs et al., 2022) and piedmont lobes (Salcher et al., 2010; Monegato et al., 2007; Preusser et al., 2011) released on the ground a large set of well-preserved moraines and landforms testifying major advances at 26.5 to

23 ka BP (Monegato et al., 2007; Wirsig et al., 2016). The size of the glacier piedmont lobes was different across sectors and not always corresponding to large accumulation areas (Ivy-Ochs et al., 2022). The largest glaciers were located in the northern and western regions of the Alps (Rhône, Rhine, Isar-Loisach, Inn and Salzach), whereas piedmont lobes were smaller to the south, with only a few exceeding 250 km2 (Ivrea, Verbano, Lario, Garda and Tagliamento). In fact, they remained confined into the valleys of the southwestern and eastern Alpine sectors (Durance and Drau were respectively the largest trunk glaciers). The LGM Alpine glaciers started their collapse not synchronously from 20 to 18 ka BP with still-stand phases and short re-advances (Monegato et al., 2017; Wirsig et al., 2016; Ivy-Ochs et al., 2004; Fontana et al., 2014; Ravazzi et al., 2014).

During the LGM, atmospheric and environmental conditions were drastically different from today. The mean sea level dropped by about 120 m (Clark et al., 2009; Lambeck et al., 2014; Yokoyama et al., 2000) as a consequence of the sustained growth of ice sheets and mountain glaciers worldwide, and this lead to the exposure of lands that were previously submerged. A typical example is the North Adriatic region, which was characterized by a transition from the semiarid Adriatic alluvial Plain to wide braided proglacial rivers in the Alpine piedmont area (Peresani et al., 2021). Global surface air temperature during the LGM was 1.7 to 8.2 °C lower than in present conditions (Schmittner et al., 2011; Annan and Hargreaves, 2013; Snyder, 2016; Tierney et al., 2020), although a large discrepancy still exists between model simulations and proxy data (Jost et al., 2005; Kageyama, et al., 2006; Ramstein et al., 2007).

During the LGM, air-masses followed different patterns compared to today, thereby modifying global and regional precipitation regimes. In particular, most model simulations (Laîné et al., 2009; Merz et al., 2015; Pinto and Ludwig, 2020; Strandberg et al., 2011) and proxy records (Monegato et al., 2017; Luetscher et al., 2015) show evidence of a southward shift of the Atlantic storm track caused by the expansion of the North American ice sheets (NAIS). Laîné et al. (2009) noted a thinning of the storm track in the north-western Atlantic associated with an intensified baroclinicity between the Azores Islands and Iberian Peninsula. This lead to a relatively wet climate in southwestern Europe and dry conditions North of the Alps. The differential insolation and temperature between the subtropical regions and the mid to high-latitudes, together with a semi-permanent blocking high over the Fennoscandian ice sheet, determined a marked latitudinal pressure gradient likely responsible for Rossby-wave breaking west of the Alps (Luetscher et al., 2015; Florineth and Schlüchter, 2000). This in turn induced a latitudinal flow of moist air from the subtropics towards the Alpine range, where air masses were forced to rise and release abundant precipitation, thus triggering ice build-up on the up-wind slopes (Monegato et al., 2017; Luetscher et al., 2015; Florineth and Schlüchter, 2000). Increased precipitation in the Southern Alps and western Mediterranean may also be ascribed to intense and frequent cyclogenesis in the Gulf of Genoa due to polar air outbreaks over the warm Mediterranean Sea (Kuhlemann et al., 2008).

The atmospheric circulation during the LGM over Europe has been widely studied (e.g., Beker et al., 2016; Ludwig et al., 2016; Kuhlemann et al., 2008; Florineth and Schlüchter, 2000). However, a large uncertainty still exists about the main mechanisms sustaining the expansion of Alpine glaciers during the LGM. The analysis of speleothems sampled in the Sieben Hengste cave system in the Bernese Alps suggests that the LGM glacier expansion was predominantly fed by precipitation

occurring between spring and autumn (Luetscher et al., 2015). Conversely, recent research (Spötl et al., 2021) relating cryogenic cave carbonates formation from Obir caves in the Northern Karawanks with precipitation and permafrost suggests that the LGM glacier advance in the Alps was determined by intense snowfalls during autumn and early winter. One of the major challenges in paleoclimatic reconstruction (from both models and proxies) is thus to reduce the uncertainties in estimated LGM precipitation patterns, especially at small spatial scales in areas of complex orography (Kirtman et al., 2013).

70 This challenge can be addressed with the use of regional climate models (RCMs), which allow one to carry out simulations at resolutions of a few tens of km, or even less (e.g. Giorgi, 2019).

Here we use the regional model RegCM4 (Giorgi et al., 2012), nested into the earth system model developed by the Max Planck Institute for Meteorology (MPI-ESM-P; Stevens et al., 2013), to investigate possible atmosphere-cryosphere interactions leading to the expansion of the LGM glaciers in the European Alps, in particular as related to the seasonality and

75 spatial variability of atmospheric circulations and associated precipitation. In this regard, in order to be consistent with the periods of available MPI-ESM-P fields providing the initial and boundary conditions to run our RCM, here the simulated LGM corresponds to 21 ka BP, the last phase of the actual LGM, which is considered the standard in paleoclimate modelling according to the PMIP3 protocol (Braconnot et al., 2012).

A glacier's sensitivity to changes in climate conditions is reflected by the Equilibrium Line Altitude (ELA), i.e. the line

80 separating the accumulation area from the ablation one (Haeberli et al., 2007; Lie et al., 2003; Mcgrath et al., 2017; Zemp et al., 2008). More precisely, the ELA is defined as the spatially averaged altitude of the set of points on the surface of the glacier where the ice mass balance is zero at a given time (Cogley et al. 2011). When the ELA is inferred at a regional scale without considering the effects of the morphology of the surface (i.e. shading, avalanching, snow drifting, glacier geometry or debris-cover) and it is averaged over at least some decades, it is called environmental ELA (envELA) which represents the

85 theoretical altitude where a glacier can form and be sustained in a region (Anderson et al., 2018). Therefore, changes in ELA are especially powerful indicators of climate-glacier interactions. Here, we estimate the envELA of Alpine glaciers at 21 ka BP and pre-industrial (PI) times following the methodology developed by Žebre et al. (2020). We calculate the envELA using a simple parametric equation based on the theory of mass and energy conservation, which relates simulated summer temperature and annual precipitation (Ohmura and Boettcher, 2018) disregarding the local topographic effects acting on

90 glaciers. An advantage of this method is that it does not require elaborate input datasets as in more sophisticated approaches which include the glacier dynamics driven by mass balance processes (e.g., Huss and Hock 2016; Zekollari et al., 2020). Finally, we assess the different contributions to the 21 ka BP glacier envELA, and in particular the concurrent action of low temperatures, reduced snowmelt and evaporation, increased southerly moist air advection towards the Southern Alps, intensified cyclogenesis in the Tyrrhenian region and convection during the warmer months.

2 Methods

2.1 Experimental Design

In our experiments we use a double nesting approach. The large-scale driving fields are produced by the Max Planck Institute for Meteorology Earth System Model in Paleo Mode (MPI-ESM-P; Stevens et al., 2013), compliant with the PMIP3/CMIP5 protocol (Paleoclimate Modelling Intercomparison Project; Braconnot et al., 2012), for two 20 years time slices extracted from 150-year-long simulations at the LGM standard (21 ka BP) and PI. Then, the International Center for Theoretical Physics RCM RegCM4 (Elguindi et al., 2014; Giorgi et al., 2012) is nested into the MPI-ESM-P model with an intermediate 50 km resolution domain, which in turn drives a high-resolution domain at 12 km grid spacing. The 20-year-long RCM data are then post-processed by removing an initial 1-year spin-up period and the four grid point wide lateral buffer zone, an area on the edge of the domain where the MPI-ESM-P forcing conditions are assimilated by the RegCM4 (e.g. Giorgi 2019).The resulting 19-year-long simulations over the interior of the domain are then used for the analysis.

The MPI-ESM-P has already been successfully employed in the study of the LGM (e.g. Pinto and Ludwig, 2020), showing an overall behavior in line with other models (Ludwig et al. 2016), while for the RegCM4 this is the first application to paleoclimate studies in the Alpine region. We evaluated both models against observations (CRU; Harris et al., 2013) and reanalysis data (ERA-Interim; Dee et al., 2011) after customising the RegCM4 and providing it with a tailored land-use reconstruction. The greenhouse gas (GHG) concentrations used in both the global and regional simulations are compliant with the CMIP5/PMIP3 protocol (Braconnot et al., 2012) for 21 ka BP and the PI conditions. The MPI-ESM-P uses orbital parameters and ice-sheet reconstruction from the same protocol, while the orbital parameters for the RegCM4 are calculated following the equation proposed by Berger (1978). Note that, even though the atmosphere and glaciers are transient systems, a 20-year-long simulation represents a relatively short interval within the longer temporal framework of the LGM and of the evolution of extended glaciers, and therefore the analysis assumes steady state conditions.

2.2 Domain of study

High-resolution RegCM4 simulations (~12 km, see methods) are carried out over a domain extending between 4 and 20 °E and 38.5 to 50 °N, which includes the Alpine and Balkan Mountain ranges in their full extent, along with the north-central Apennines. However, our focus for the envELA calculations is on the Greater Alpine region (~4 to 16°E and ~43.5 to 48.5°N), where bias correction is applied to temperature and precipitation data produced by RegCM4 (Eqs. 1, 2) based on two observational datasets covering this area.

2.3 Land-use and topography reconstruction

During the LGM, the land surface conditions were quite different from present, and this information needs to be fed into the model, as it may affect the regional climate (Ludwig et al. 2017). These conditions may be reconstructed using available proxies and paleoclimate archives. First, for LGM conditions we modified the present-day model topography (GMTED2010;

Danielson and Gesch, 2011) and bathymetry (ETOPO1; Amante and Eakins, 2009) by decreasing the sea level by 120 m (Peltier and Fairbanks, 2006), and changed the land sea-mask in order to account for the corresponding variation of the coastline. The resulting dataset was then interpolated by the RegCM4 preprocessor tool onto the desired grids at 12 and 50 km. This caused a smoothing of the topography that in particular affected the smallest orographic features, such as mountain tops and narrow valleys. Finally, we added a two-dimensional representation of the LGM glaciers based on Ehlers et al. (2011). Because of the topography smoothing and the relatively coarse RegCM4 resolution, the Alpine glacier thickness is not considered in the topography representation, although Merz et al. (2015), Imhof (2019) and Velasques et al. (2022) highlighted the importance of including glaciers' topography into global and regional paleoclimate models. Concerning LGM vegetation cover, we constructed a high-resolution dataset based on proxy data (Monegato et al., 2015; Duprat-Oualid et al., 2017), using an association of plant types in each region with altitude and latitude, modulated by a random spatial distribution within each region. Every plant type is characterised by an annual cycle in leaf and steam area index.

2.4 Bias correction

In order to account for model biases in the PI simulation (e.g., a precipitation overestimation over the Alps), we applied a first-order bias correction to precipitation and temperature output data. We first calculated the bias by comparing observations and pre-industrial RegCM4 data for both variables. Then we applied a correction to the RegCM4 PI and 21 ka BP temperature and precipitation, assuming that the biases between model and observations are the same in the two time periods. Precipitation is thus corrected by applying a linear scaling approach:

$$P_{corr} = \frac{P_{y,LAPREC}}{P_{y,PI}} * P_{y,RCM}, \tag{1}$$

where $P_{y,LAPREC}$ is annual accumulated precipitation from the LAPrec observation dataset (Auer et al., 2007; Isotta et al., 2014) averaged over the period 1871-1900, $P_{y,PI}$ is annual accumulated precipitation from the pre-industrial RegCM4 simulation averaged over 19 years, and $P_{y,RCM}$ is the simulated annual accumulated precipitation (PI or 21 ka BP) which needs to be corrected. Similarly, temperature is corrected as:

$$T_{corr} = T_{m,RCM} + (T_{m,PI} - T_{m,HIST}), \tag{2}$$

where $T_{m,RCM}$ is the simulated summer monthly mean temperature (PI and 21 ka BP) that we want to correct, $T_{m,PI}$ is the summer monthly mean temperature from the PI RegCM4 simulation averaged over 19 years, and $T_{m,HIST}$ is the summer monthly mean temperature from HISTALP dataset (Auer et al., 2007) averaged over the period 1871–1900.

2.5 Environmental Equilibrium Line Altitude

We calculated the envELA defined as the regional altitude of zero mass balance determined only by climatic factors (Anderson et al., 2018). The envELA is calculated following an inverse approach based on bias corrected annual precipitation and summer temperature (Eqs. 1 and 2) and is averaged over the 19 years of the model simulations, since we

assume that glaciers are at a steady-state during the simulation time. The calculation uses the methodology adopted by Žebre et al. (2020) which is based on an empirical equation relating mean summer temperature and accumulated annual precipitation at the envELA. This equation relates glacier and climate conditions; it was first introduced by Ahlmann (1924) in the form of a precipitation/temperature diagram (P/T diagram) and then recently updated by Ohmura and Boettcher (2018)

160 using temperature, precipitation and solar radiation data from 104 glaciers worldwide. The P/T curve can be approximated by a quadratic function and is based on the principles of mass and energy conservation:

$$P_{corr19} = 5.87 * T_{ELA}^2 + 230 * T_{ELA} + 966 \tag{3}$$

Equation (3), representing the P/T diagram, is solved for T_{ELA}, using P_{corr19}, which is the RegCM bias-corrected accumulated annual precipitation averaged over the 19 years. Proceeding with an inverse approach, we assume that only precipitation

165 (P_{corr19}) refers to the envELA level, but not temperature. Then, we use bias-corrected RegCM precipitation (P_{corr19}), assumed at the envELA, to calculate with Eq. (3) the envELA temperature (T_{ELA}). Subsequently, we convert the temperature difference between the envELA and the topography ($T_{ELA} - T_{corr19}$) into an altitude difference, using an environmental lapse rate of 0.65°C 100m^{-1}. Finally, the resulting elevation difference is subtracted from the topography (DEM) in order to obtain the envELA for every grid-cell (Fig. S1), as

170 $$envELA = DEM - \left[\frac{(T_{ELA} - T_{corr19}) * 100}{0.65} \right] \tag{4}$$

A further assumption implicit in this approach is that temperature varies vertically but not precipitation.

The reference topography for the 21 ka BP and PI envELA calculations is the PI topography, after the application of a correction accounting for the 120 m of elevation difference between the two periods due to the sea level decrease. This facilitates the comparison of the envELA datasets for the two periods and with the ELA values obtained from

175 geomorphological reconstructions. The envELA computations for both the 21 ka BP and the PI are performed using three different topographies, the RegCM4, the HISTALP, and LAPrec ones. The three resulting envELA datasets are then averaged. Because the observational and simulated datasets do not use the same horizontal grid, we remapped the RegCM4 and LAPrec data onto the HISTALP 5 arcmin resolution grid.

This method has already been validated for the Alpine region by Žebre et al. (2020) using two different ELA datasets: i) the

180 Fluctuation of Glaciers (FoG) database of the World Glacier Monitoring Service (WGMS), from which geographically and climatologically distributed end-of-mass-balance-year ELA values over the Alps were selected for the period 1948 – 2017; and ii) the annual highest end-of-summer Snow Line Altitude (SLA) derived from Landsat data for the western Alps for the period 2006-2019, which was analysed using a semi-automated remote sensing method (Racoviteanu et al., 2019).

For the sake of clarity we ephasize that the envELA is the lowest boundary of the climatic glaciation, and therefore areas

185 where the envELA is lower than the model topography indicate conditions (RegCM4 precipitation and temperature) supporting the existence of glaciers.

3 Results

3.1 The large-scale framework: the MPI-ESM-P simulation

The MPI-ESM-P global model run at the Max Planck Institute, is used to drive our RegCM4 simulations (see methods). This model (not shown in figure) was already analysed in other studies (e.g., Ludwig et al., 2016) and correctly reproduces the large-scale conditions at 21 ka BP in terms of jet-stream position and strength, temperature and precipitation anomalies. The 21 ka BP European climate simulated by the MPI-ESM-P is on average 9 °C colder and overall drier than at PI time over our broad region of interest, particularly over central and northern Europe (−30 %). The southern flank of the Alps, however, is somewhat wetter than, or with similar precipitation levels as, at PI time. The main upper troposphere circulation over the area of interest is westerly and north-westerly, both at 21 kaBP and PI. The 21 ka BP-minus-PI anomaly in the MPI-ESM-P model highlights a southward shift of the Atlantic jet stream, which at the 21 ka BP generated strong winds in the Mediterranean region. The Scandinavian Ice Sheet at the 21 ka BP generated a semi-permanent high-pressure system responsible for blocking and deflecting the westerly air masses around the southern margin of the Ice Sheet.

3.2 Regional Climate Model RegCM4: Atmospheric circulation

3.2.1 Synoptic conditions

The 21 ka BP high-resolution RegCM4 simulation shows the presence of a more pronounced NE-SW pressure gradient compared the PI, with a maximum in the northeastern sector of the domain and a minimum over the Tyrrhenian and the Mediterranean Sea, particularly evident in the coldest months (Fig. 1). A similar pattern is shown by the annual temperature anomaly, with lower values northeast of the Alps and higher values over the Tyrrhenian region (Fig. 2). The largest temperature anomaly between the 21 ka BP and PI occurs in winter (−8.30 °C on average), especially northeast of the Alps and in the northern Adriatic. During winter, the monthly mean anomaly is smaller in the Alpine region than in the rest of the domain, while during summer the anomaly is larger over the Alps.

The 700 hPa winds (Fig. 1) indicate that in the at 21 ka BP during winter the Tyrrhenian region is characterised by advection of cold air descending the Italian peninsula from the northwest. The PI shows a similar pattern in the southern part of the domain, but north of the Alps the main wind direction presents a more zonal component. During the warmer months at 21 ka BP the air masses coming from the northwest are deflected eastward over the Tyrrhenian Sea. This often generates a cyclonic circulation over the Gulf of Genoa which occasionally leads to a north-easterly flow. At the PI the average summer flow does not show this north-easterly curvature but is east-southeast oriented. Generally, south of the Alps the circulation is stronger at the 21 ka BP than at PI, while north of the Alps it is weaker.

3.2.2 Temperature, precipitation and winds

Compared to the PI time, the simulated LGM conditions are colder, with a lower average temperature of ~6.6°C (Fig. 2) and annual precipitation reduced by ~16.4% (Fig. 3) over the Alps. Despite the overall drier conditions characterizing the LGM, we find some relatively wetter areas in the southeastern Alps, the Dinaric Range, the Ticino region, and the northern Apennines (Fig. 3). The RegCM4 simulations thus highlight the important role played by the Alpine orography, which determines two distinct climate regimes north and south of the Alps. At the 21 ka BP, Central Europe is 20 to 40 % drier than at PI, while the southern Alpine flanks present some wetter areas (up to 20%) during the simulated LGM.

The use of RegCM4 allows us to distinguish between convective and stratiform precipitation. The former dominates during the warmer months, over the sea and at the lowest elevations, but shows a marked reduction in the at 21 ka BP due to the lower temperatures. For example, in central Europe and over the Alps convective precipitation in the at 21 ka BP is reduced by about 50% compared to the PI. Conversely, stratiform precipitation deriving from larger scale circulations presents positive anomalies in the at 21 ka BP compared to PI almost everywhere and year-round. In the Alpine region during the PI, convection is always dominant, while at the 21 ka BP it dominates only during summer. The yearly maximum of stratiform precipitation over the Alps corresponds to the maximum of total precipitation, which occurs in September. Our data also shows increased 21 ka BP cyclonic activity compared to the PI in all seasons over the Italian peninsula.

In Figure 4 we analyze wind direction and associated precipitation for four subdomains corresponding to LGM Alpine piedmont glaciers: the Rhine and Inn-Salzach-Traun glaciers in the northern Alps, and the Dora Baltea and Tagliamento glaciers in the southern Alps. We used daily data from the 19 simulated years in order to calculate the frequency and intensity of precipitation associated with given wind directions. The two glaciers north of the Alps are mainly affected by precipitation brought by north-westerly and westerly air masses. At 21 ka BP, north-westerly winds dominate, especially in summer, while at the PI, westerlies occur more frequently. At 21 ka BP, more precipitation events are low intensity (darkest blue in Fig. 4), as northerly and north-westerly (dry) winds reach the northern rim of the Alps. In the southern Alps, the Dora Baltea and Tagliamento glaciers present quite different precipitation and wind patterns. The Dora Baltea glacier is affected mainly by winds from the northwest and southwest, however, the events from the west and northwest are often dry, while the most intense precipitation comes from the southwest and southeast.

The southern Alps at 21 ka BP receive much more precipitation than the northern Alps. The Tagliamento glacier is shielded by the Alpine topography barrier from precipitation coming from the northern and eastern quadrants, while precipitation is supplied by south-westerly winds. This precipitation is more abundant at 21 ka BP than at the PI (Fig. 4 and Fig. S2) and the frequency of intense precipitation is the highest across the domain. At 21 ka BP, precipitation associated with south-westerly air masses is intense throughout the year, which is an important difference compared to the glaciers in the northern rim of the Alps showing only one rainy season (JJA).
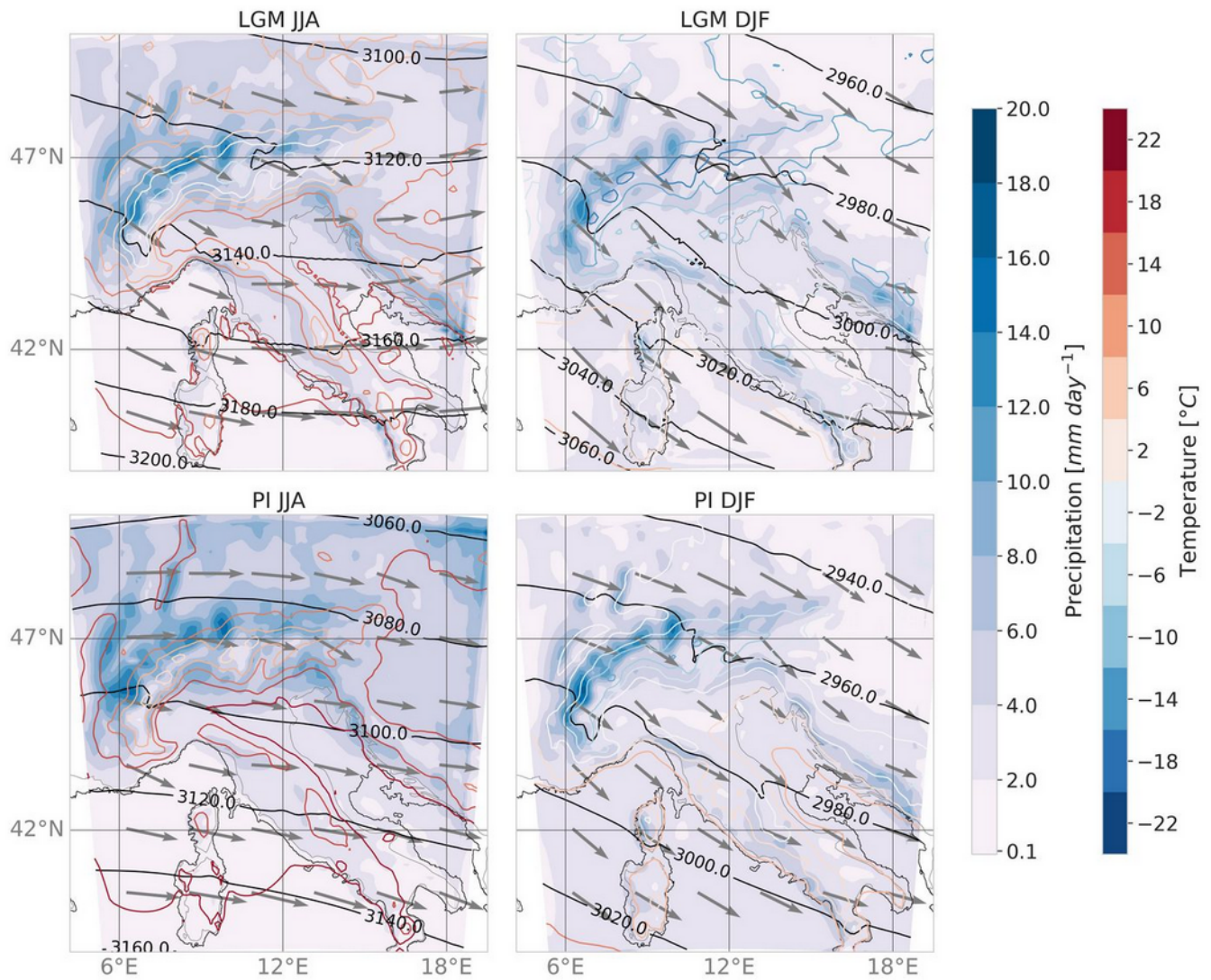
Figure 1: 21 ka BP and PI mean summer and mean winter synoptic conditions averaged over 19 years. 21 ka BP 700 hPa average wind field (arrows), temperature (blue to red lines), precipitation (blue scale) and 700 hPa geopotential (black lines). Temperature and precipitation are not bias-corrected. These data represent the average summer and winter situation.

250
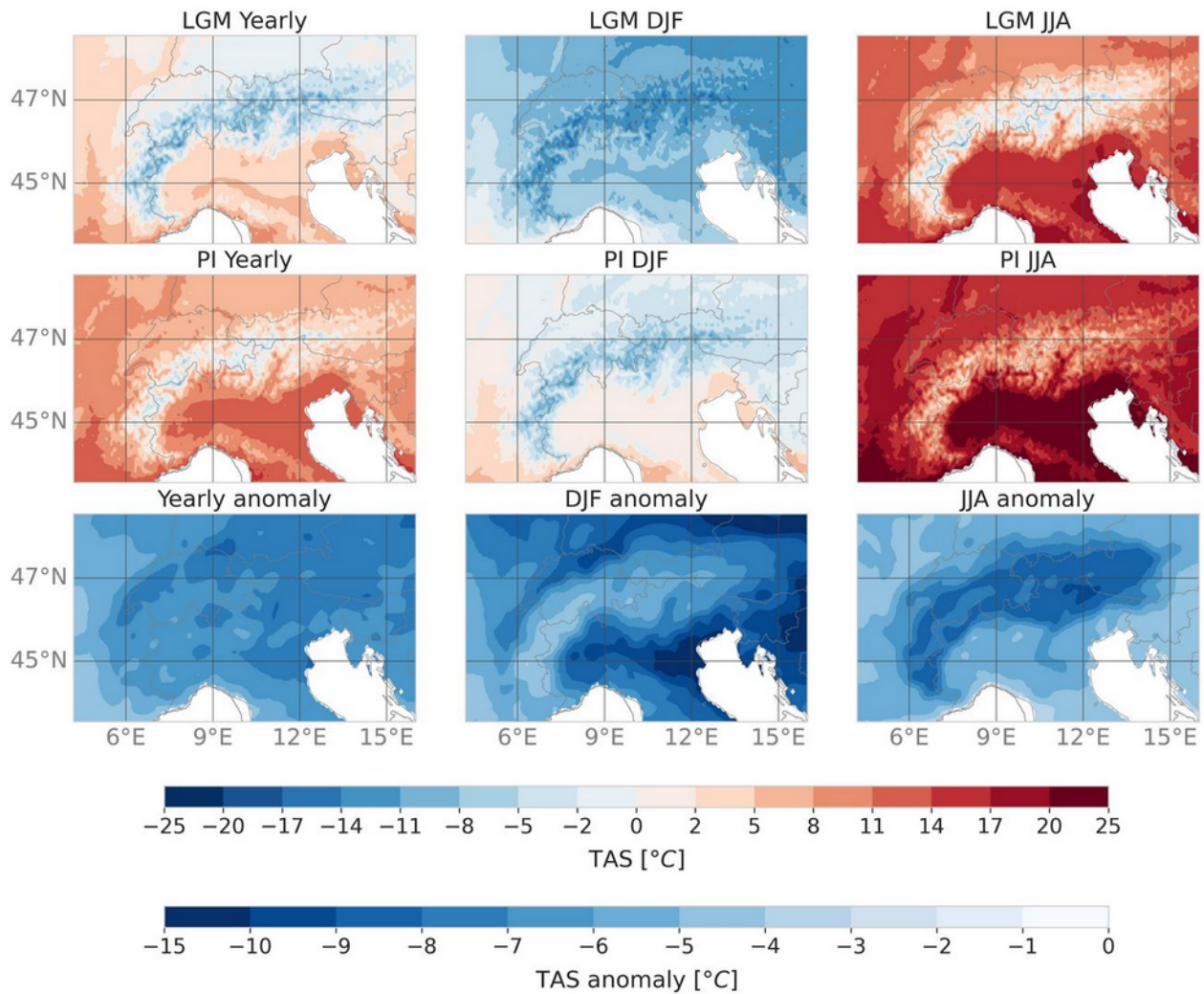
Figure 2: 21 ka BP and PI temperature and anomaly. Yearly, winter and summer averaged over 19 years-long RegCM4 bias-corrected temperatures data.
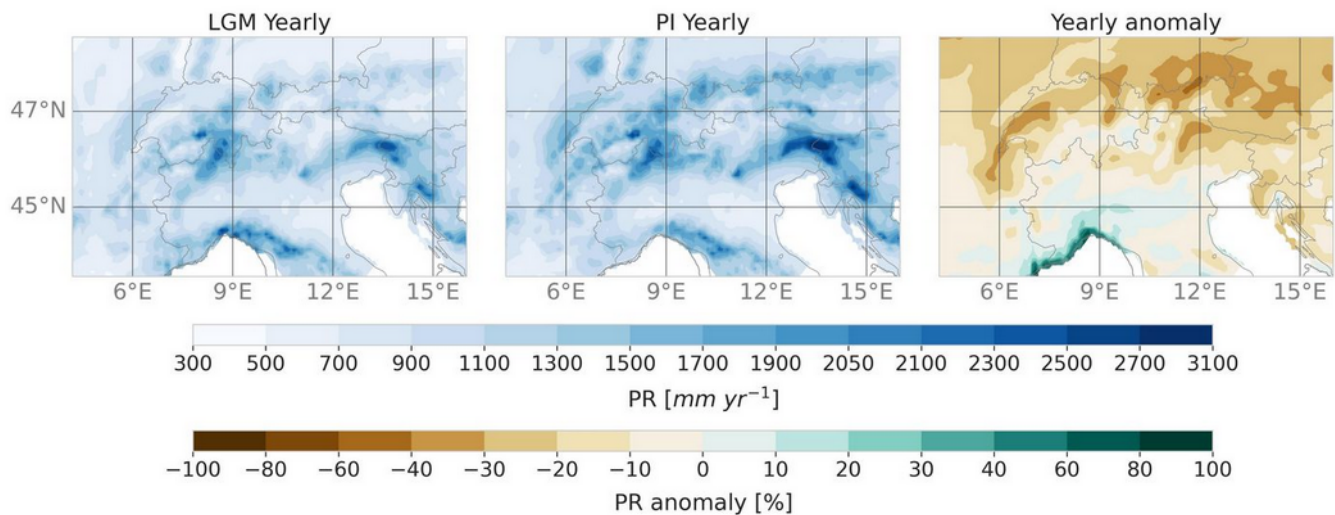
255

Figure 3: 21 ka BP and PI precipitation and anomaly. Yearly averaged over 19 years-long RegCM4 bias-corrected precipitation data.

3.3 Equilibrium Line Altitude

The envELA calculations were performed following the method proposed by Žebre et al. (2020) (Eqs. 3, 4, see methods). At
260   21 ka BP over the greater Alpine region the average envELA is 1444 m a.s.l. (Fig. 5), while at the PI is 2435 m a.s.l. (Fig. S3), i.e. there is a drop of 991 m at 21 ka BP (Fig. S4). The south-western and north-eastern Alps show the highest envELA values, while the Ticino, south-eastern and the rest of northern Alps present the lowest values both at 21 ka BP (Fig. 5) and PI (Fig. S3). The calculated 21 ka BP envELA is between 1000 and 1250 m a.s.l. over the Julian Alps, between 1250 and 1750 m a.s.l. in the Pennine and Graian Alps and between 1500 and 2250 m a.s.l. in the Maritime Alps. In the western Alps,
265   the envELA decreases northward, in central Alps it is lower on the southern rim because of high precipitation in the Ticino region, while in the eastern Alps no significant north-south gradient in envELA is found.

By comparing the envELA with the model topography (Fig. S5, S6) we can investigate whether the RegCM4 is able to reproduce the correct combination of temperature, precipitation and orography to support the existence of glaciers. At the PI only few grid-cells in the western Alps show an envELA lower than the model topography, while the 21 ka BP envELA is
270   lower than the topography over a large section of the Alps, falling within the reconstructed glacier front (Ehlers et al., 2011). The RegCM4 simulations also allow us to investigate the different elements affecting the hydrological and glaciological cycles. The lower 21 ka BP temperatures lead to longer winters with a consequent more abundant snow amount on the ground lasting until May over most of the Alpine region. Minimum snow amounts over the Alps are reached between August and September, when the first abundant snowfalls end the melting season. Despite the lower temperatures, the 21 ka BP
275   snow melting is important due to the large amounts of snow persisting throughout the summer and leading to a permanent snow limit at about 1300 m a.s.l.
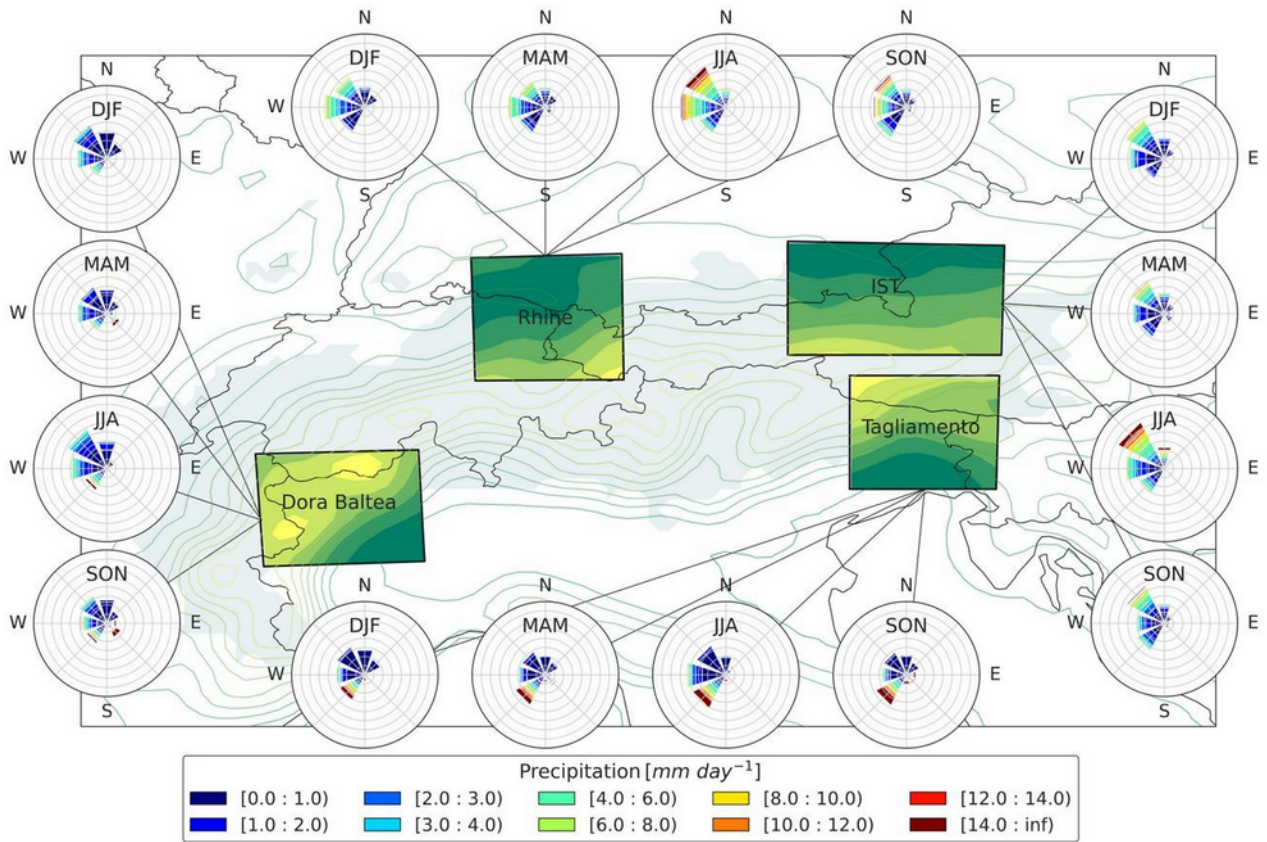
Figure 4: 21 ka BP wind origins and associated precipitation for four alpine glaciers. Seasonal windroses and precipitation intensity frequency associated to every wind event of the 19 simulated years for Rhine, Inn-Salzach-Traun (IST), Tagliamento and Dora Baltea glaciers. Precipitation is daily cumulated. The shadow in the map is the glacier extension (Ehlers et al., 2011), the color lines as well as the full color in the boxes represent the topography (yellow for higher elevation and green for the lowers) and the black line is the present-day political boundary.
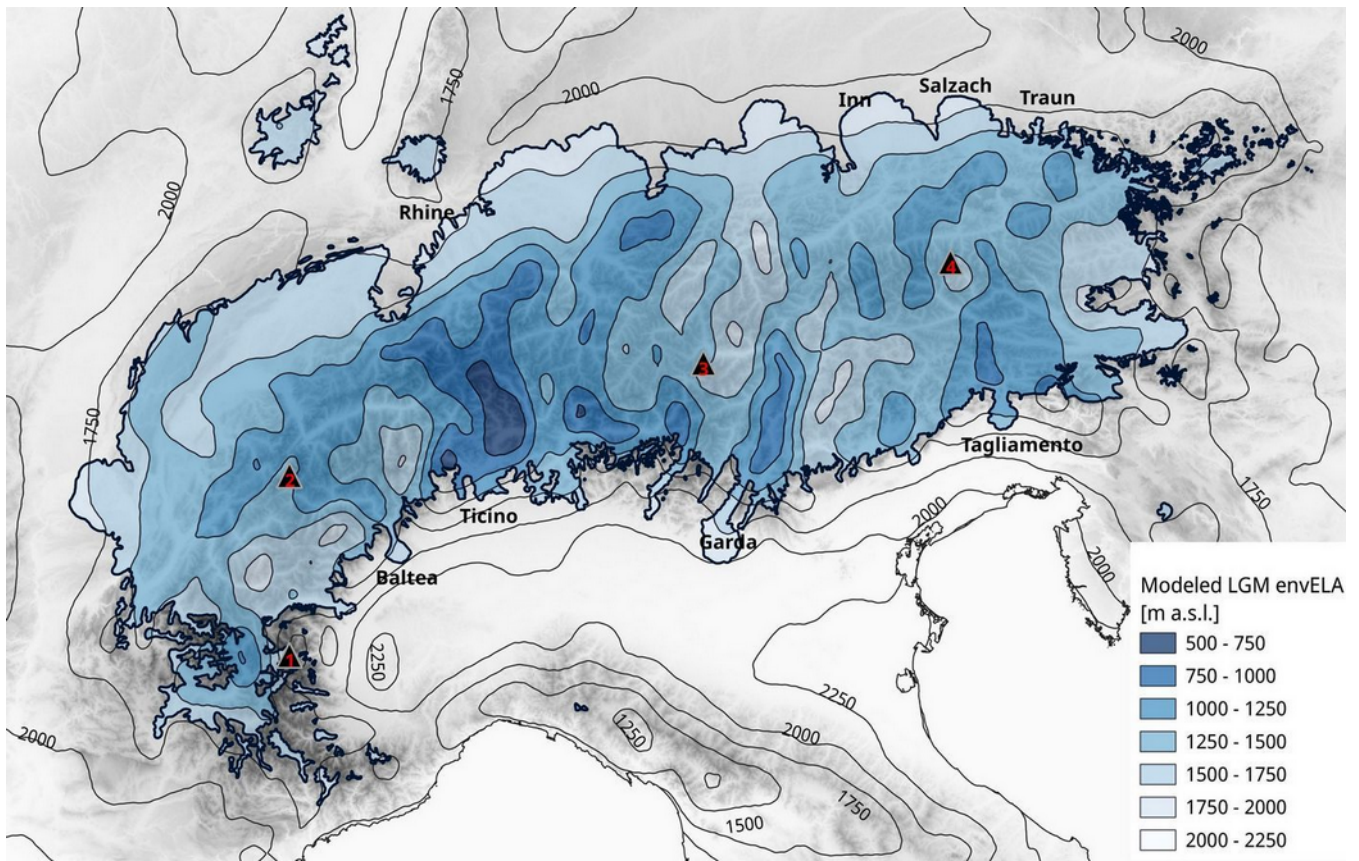
Figure 5: 21 ka BP envELA. Env ELA calculated following the method of Žebre et al. (2020), with the extension of the geomorphological reconstruction of the LGM glaciers (Ehlers et al., 2011). The black triangles indicate: 1) Monviso, 2) M. Blanc, 3) Ortler, and 4) Großglockner.

4 Discussion

4.1 EnvELA - comparison with other studies

The model resolution here presented is among the highest found in paleoclimate studies (Imhif et al.,2021; Ludwig et al., 2021; Velasquez et al., 2020; Velasquez et al., 2021). Therefore, the simulations provide more detailed information about PI and 21 ka BP climates compared to the MPI-ESM-P, particularly concerning the effect of complex topography. After a bias correction is applied to the model output using present day observations, the precipitation and temperature patterns for the 21 ka BP show good consistency with proxy records (Bartlein et al., 2010; Wu et al., 2007; Duprat-Oualid et al., 2017; Monegato et al., 2015; Sirocko et al., 2016; Tzedakis, 2005; Watts et al., 1996) and other RCM studies (Strandberg et al., 2011, Ludwig et al., 2021; Kageyama et al., 2020; Stadelmeier et al., 2021).As such, the used modeling system highly improved the capabilities of capturing the basic regional climate response during the LGM. In fact, envELA reconstruction

(Fig. 5) compares well with other local estimations for the LGM (e.g. Kuhlemann et al., 2008; Monegato, 2012; Rettig et al., 2021; Federici et al., 2017; Cossart et al., 2012).

Previous model-based studies providing extensive reconstructions of Alpine glaciers at the LGM directly model glacier behaviour considering dynamics and ice rheology (Becker et al., 2016; Seguinot et al., 2018; Višnjević et al., 2020). Conversely, our method is based on an empirical equation which calculates the envELA from temperature and precipitation (Ohmura and Boettcher, 2018) and therefore from the glaciological point of view it is simpler than a glacier-model-based approach. Nevertheless, input data simulated with an RCM are more physically-based and specific for the Alpine region.

The reconstruction of higher envELA in the eastern and south-western Alps, which has not yet been fully resolved in previous studies (Becker et al., 2016; Jouvet et al., 2017; Seguinot et al., 2018; Višnjević et al., 2020). is more consistent with geomorphological evidence. According to geomorphological records (Ehlers et al., 2011), in these two sectors, hosting the Mur, Drava, Durance, and the Maritime Alps glaciers, a previous model-based reconstruction (Seguinot et al., 2018) apparently overestimated the glaciation by tens of kilometers. Likewise, underestimation of the glacier extent were also found in previous studies for the Rhône Glacier complex, the Jura Mountains, the Lyon Lobe, the Adda, the Garda and the Piave sectros (Seguinot et al., 2018). Our results show a drop of the envELA in these sectors, which is definitely more consistent with the geological reconstructions (Ehlers et al., 2011) (Fig. 5).

Similarly, the application of a constant climate forcing to an ice-flow model (Becker et al.; 2016) produced simulated glacier extents not consistent with the geological reconstructions of LGM moraine systems in the northern, eastern, and western Alps, although this model captured the meridional shift of the precipitation patterns across the Alps.

Using high resolution envELA information, as it has been done in this climate-based modeling study, can therefore integrate the understanding of glacier cycles and extent in the Alps. Infact, our paleoclimate simulations describe with high detail the zonal and meridional temperature and precipitation gradients implied by the envELA calculations. Despite the different time responses of envELA and glacier extention to changes in climate, since the envELA is directly related to temperature and precipitation while the glacier extention has a lag due to ice dynamics, according to Žebre et al. (2020) the envELA variations can be associated with variations of the front position and the effective ELA of glaciers (i.e. the ELA calculated from geodetic or direct glaciological mass balance measurements). Also, the envELA calculations allow a more detailed discussion of local differences in the geological reconstructions over the Alpine region.

4.2 Limitations and consideration about the experimental set-up

We stress that the results would still be limited by uncertainties in the driving large scale climate forcing and by the intrinsic complexity of the glacier mass balance processes. For example, the ELA distribution is determined by multiple factors that still cannot be entirely disentangled and represented with a model, e.g. avalanches, wind drifts, dust deposition, or debris fraction. A further uncertainty in the envELA calculations is due to liquid precipitation, which represents a potential mass loss (Žebre et al., 2020). As a matter of fact, our method calculates the envELA only from climate fields, which can provide an accurate information considering the whole Alpine chain but cannot capture effects related to local topo-climatic

330 conditions. As we are interested in the climate fields, the steady state assumption and the ELA averaging over the whole simulation time masks the effects of outlier anomalous years. Indeed, as shown by Žebre et al. (2020), a year-by-year envELA computation would reflect these events. Conversely, the effective ELA does not react quickly to extreme events, being the result of snow accumulation and metamorphism also from previous years. In this framework, the envELA averaged over the 19-years of our simulations can provide a more reliable estimation of the effective ELA in terms of

335 absolute values and temporal evolution. In fact, Žebre et al. (2020) pointed out that the envELA averaged over a long climate period shows a good match with the effective ELA of glaciers particularly susceptible to avalanches and wind-blow snow. Thus, the steady-state assumption enables us to at least reduce part of the deviation between effective and environmental ELA. On the other hand, the steady-state assumption implies that the dynamical and transient aspects of climate-glaciers interactions are overlooked.

340 Our LGM simulation refers to 21 ka BP. This time does not correspond to the maximum glacier extention during the LGM, which occurred between 26.5 and 23 ka BP, although individual Alpine glaciers reached their maximum extent and started their retreat at different times in different sectors (Monegato et al., 2017; Seguinot et al., 2018). Because at 21 ka BP the withdrawal of the Alpine glacier had not yet started we assume that 21 ka BP is a good approximation for average conditions during the LGM. In particular, radiocarbon and cosmogenic isotope datings (Ivy-Ochs et al., 2022; Kamleitner et al., 2022)

345 show a late retreat (~18 ka) for some glaciers in the southern Alps (Garda and Ticino), for which our calculations indicate a low envELA (Fig. 5), while the Dora Riparia, Dora Baltea, Piave and Tagliamento glaciers started withdrawing earlier.

A possible uncertainty in our results is related to the model resolution and glacier thickness. In particular, the latter can modify not only the temperature patterns but also precipitation and wind fields. Due to the topography smoothing in the RegCM4 and the model relatively coarse resolution we did not include ice thickness in the simulations. However, where the

350 valleys are larger (Garda and Rhône) this might introduce some uncertainty in the envELA estimations. The RegCM4 cannot capture the multitude of small glaciers present at the PI over the whole Alpine region but can identify areas where the envELA is lower than the model topography, which occur mostly in the western Alps (Fig. S6). Conversely, at 21 ka BP the larger glacier systems are better captured by the model (Fig. S5).

4.3 Links between glacier behaviour and topography

355 Our results suggest a particularly low envELA (750-1250 m a.s.l.) in the Rhine, Rhone and Ticino valley knot (Fig. 5) where the Rhine and Rhone ice domes are located (Kelly, et al., 2004) at an elevation higher than 4000m a.s.l.. To the south, the reconstructed glaciers originated from a largely glaciated area (about 5500 km2) including the Verbano and Ossola branches, with contributions from the Rhône glacier in the northern Alps (Kamleitner et al., 2022; Preusser et al., 2011; Scapozza et al., 2014). These glaciers' accumulation basin is asymmetric and characterized by an elevated (>4000 m) Ossola valley and a

360 large but lower elevated Ticino valley network. A low envELA (Fig. 5) is common between the Ossola and Verbano glaciers as well as the Rhône and Rhine glaciers, which formed, to the north, the largest piedmont lobes of the Alps. The northern Alpine glaciers were often characterized by large lobes with respect to the accumulation basins, while in the southern and

eastern Alps the piedmont lobes are smaller, but with large basins (Dora Baltea, Ticino, Adda, Adige-Sarca, Drau). The asymmetry of the glaciers' lobe between the northern and southern Alps is evident also in Fig. S5, where we show only the grid-cells where the envELA lies below the topography, i.e. where the model supports the formation and maintenance of a glacier. The LGM glacier extent reconstructed by Ehlers et al. (2011) in the northern Alpine foreland is much farther from the lowest glaciated areas than in the southern Alps as a consequence of topography, accumulation basin and climatology driving the development of the piedmont lobes.

By comparing our results with Seguinot et al. (2018) and Beker et al. (2016), it emerges that the distribution and dimension of Alpine glaciers is determined by a multitude of factors which also regulate the ELA distribution. Thus, it is not straightforward to associate accumulation basin dimension and elevation with the ELA distribution. This can help us to understand the discrepancies between palaeoglaciological models and ground-based data.

4.4 EnvELA and geological reconstructions

In the Julian and Carnic Alps our envELA calculations indicate values at 21 ka BP of about 1000-1250 m a.s.l. (Fig. 5), which are consistent with reconstructions spanning the range of 1130 to 1300 m a.s.l. (Kuhlemann et al., 2008; Monegato, 2012; Rettig et al., 2021). In the Pennine and Graian Alps our estimates are in the range of 1250 to 1750 m a.s.l., with good consistency with the values of 1500 m a.s.l. found by Forno et al. (2010). Our data show a particularly high envELA (2000-2250 m a.s.l.) in the Monviso area, characterized by high elevation (3841 m a.s.l.) but small LGM glaciers. In the Maritime Alps our envELA is between 1500 and 2250 m a.s.l., matches with the range values of 1685 to 1845 m a.s.l. proposed by Federici et al. (2017).

The envELA estimates for the PI (Fig. S3) can be compared with different studies of the Little Ice Age (LIA). For example, Colucci (2016) placed the ELA in the Julian Alps at 2275 m a.s.l. for the Canin glacier and at 2486 m a.s.l. for the Triglav glacier, while our results yield lower values of 1750-2000 m a.s.l. The ELA in the Ecrins group and Maritime Alps has been estimated at 3000-3100 m a.s.l. and 2841-2818 m a.s.l. respectively (Federici et al., 2017; Cossart et al., 2012), in agreement with our results of 2750-3000 m a.s.l.. Our estimate for the envELA in the Val Viola area, Central Italian Alps, is in the range of 2500-2750 m a.s.l., while Scotti et al. (2017) place it at 2815-2850 m a.s.l. It is important to stress that the envELA calculated here is based on temperature and precipitation only and is completely independent of the local physiography of the glacier's site, while the reconstructions take into account local geomorphological evidence and are site-dependent. This may at least partially explain the differences between our estimates and the reconstructed ones. Discrepancies with field reconstructions could also depend on dust, cloud cover and more in general on radiation-related fields, which are not taken into account in this work.

The decrease in envELA at the LGM compared to PI (Fig. S4) averaged over the Alpine region is 991 m, which is close to the values of 996 and 1000-1200 m suggested by Federici et al. (2017) and Ivy-Ochs et al. (2006), respectively. The western and eastern Alps (east of about 13°E) show smaller envELA decreases, mostly lower than 1000 m, while in the central Alps (western of 13°E) the decrease ranges between 1040 and 1126 m. This longitudinal gradient is in agreement with values

provided by Federici et al (2017) and Ivy-Ochs (2006). In particular, paleo reconstructions show that in the southern Alps there was a substantial decrease of envELA over the Tagliamento glaciers and in the Ticino region. Differently from Višnjević et al. (2020), in the central Alps we find a north-south ELA gradient, with the ELA increasing from south to north, while in the eastern Alps there is almost no gradient, and in the western Alps the ELA decreases from west to east. This

400   result may be explained by the seasonality of precipitations in the different sectors (Fig. 4) driven by the annual shifting of the Polar front.

4.5 Atmospheric circulation

At 21 ka BP the Alps essentially separated the dry and cold central Europe from the milder and relatively wetter southern Alpine region (Figs. 2, 3). The RegCM4 simulations suggest that the reduced precipitation in the northern Alps during the

405   LGM was caused by lower temperatures inhibiting convection and by the southward displacement of the North Atlantic storm track, the main source of moisture for Europe. In this area we also find reduced westerly winds as well as increased north-northeasterly winds (Fig. 1, 4, S2), which are eventually caused by the anticyclonic circulation triggered by the permanent high-pressure system over the Scandinavian Ice Sheet and are also responsible for enhanced dust storm activity and loess deposition (Schaffernicht et al., 2020).

410   The southern portion of European region is characterized by increased wind activity particularly over the Mediterranean areas, with meridional flows during winter and zonal flows during summer (Fig. 1). These average patterns possibly reflect the influence of seasonal variations of the polar front position. Winters show dominant northwesterly winds driven by enhanced meridional geostrophic circulation due to the marked temperature and sea level pressure gradients between the northern and southern parts of the domain at 21 ka BP. Conversely, the warmer months are characterized by a more frequent

415   cyclonic circulation over the Gulf of Genoa, which leads to northeasterly winds.

When cold polar air crossing the western Alps reaches the warmer Tyrrhenian Sea, the thermal contrast destabilizes the lower troposphere, leading to the development of lee-side cyclonic circulations and convective phenomena (Kuhlemann et al., 2008) along a storm track extending in the eastern-northeastern direction. Our 21 ka BP RegCM4 simulations, in agreement with Lutcher et al. (2015), indeed, show high precipitation rates from May to September on the up-wind side of

420   the circulations with respect to the Mediterranean jet in the Apennines, Balkans, and southern Alps. These regions, despite their low latitude, low elevation, and southern exposure, during the LGM hosted several glaciers. In particular, the Tagliamento glacier (Fig. 5) received heavy precipitation from the southwest, at higher rates during the warmer months. In addition, also during the colder months, lee-side cyclones in the Tyrrhenian Sea led to heavy precipitation in the southern Alpine slopes (Fig. 6). In the southern Alps at 21 ka BP stratiform precipitation originated from a cyclonic circulation

425   prevailing during the coldest months and at the highest elevations, while in summer, convection was more frequent, often in the form of snowfall. This type of precipitation plays a critical role in preserving the glacier from summer melting and lowering the ELA.
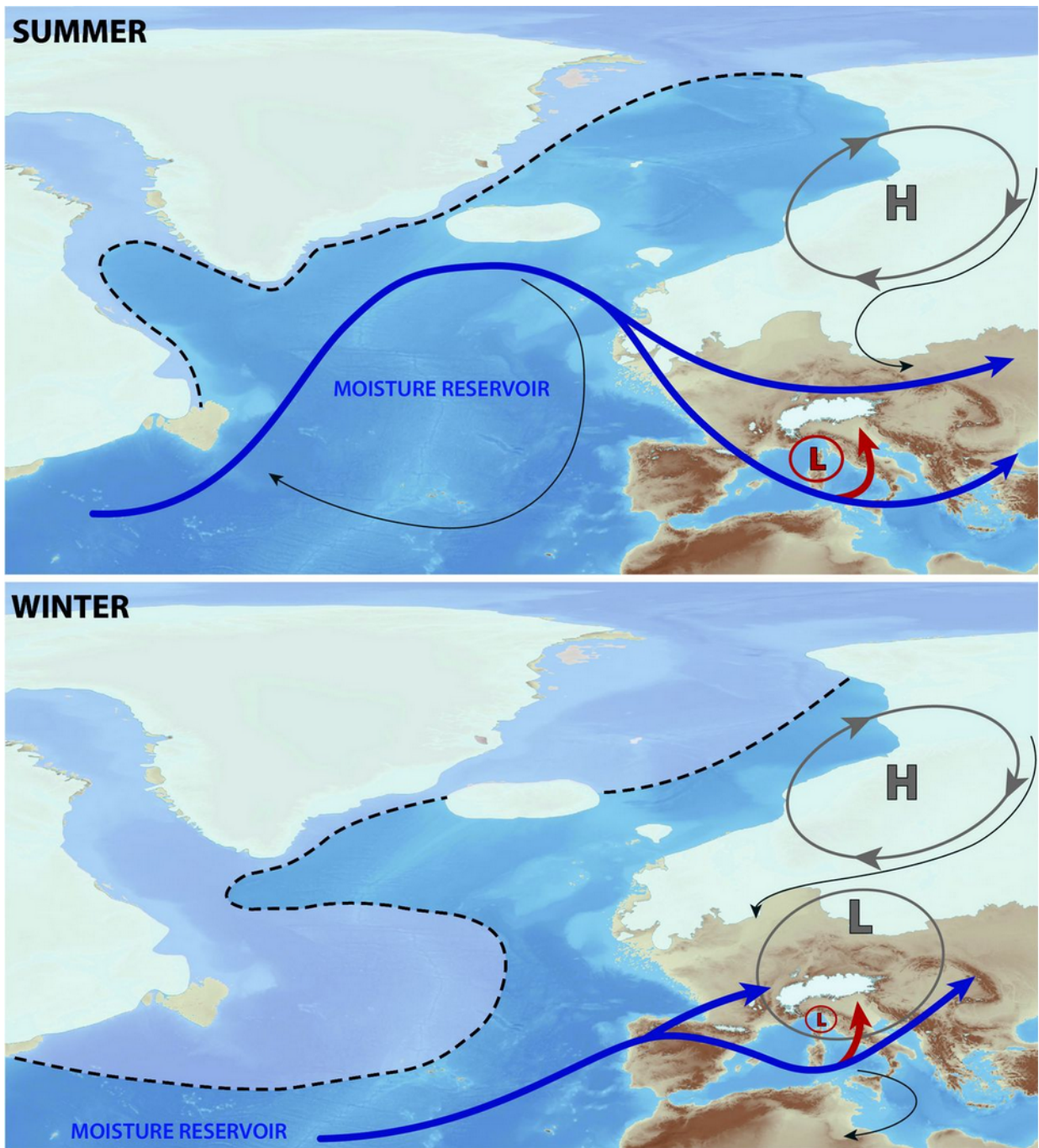
Figure 6: Conceptual model of the air masses yielding precipitation in the Alps at 21 ka BP. In white glaciers and ice sheets; the black line marks the 50% sea ice concentration extension (Rhines and Huybers, 2014); H and L stand for high-pressure and low-pressure system; blue and red arrows represent the air masses leading precipitation on the Alps; gray lines represent other air masses not leading precipitation on the Alps. Blue and gray arrows are extrapolated from the mean winter and summer MPI-ESM 850 hPa winds; while the red symbols show the elements that emerged from the RegCM4 simulations.

The mechanism suggested by our simulations is that at 21 ka BP a well-defined southerly displacement of the westerlies led
435 to a colder and drier central Europe and a relatively wetter southern European region. The envELA over the Alps was substantially lowered, with values increasing from south to north over the central Alps. Such a pattern is sustained by increased summer snowfall often reaching low elevations and feeding the Alpine glaciers. In the southern Alpine region, summer precipitation was mainly of convective origin, while during the rest of the year stratiform precipitation prevailed, often originating from a cyclonic circulation that developed over the Tyrrhenian Sea. In the northern Alps, precipitation was
440 modest and occurred mainly in summer when the polar front moved northward and some limited convection occurred.

Wind direction and associated precipitation (Fig. 4) suggest that a change of the moisture reservoirs position between summer and winter at 21 ka BP (Fig. 6) likely drove the precipitation patterns in the northern and southern Alpine regions and consequently controlled the glacier dynamics (Fig. 5). In the southern Alps the humidity was provided mainly by the Mediterranean Sea which, being relatively warm and ice-free also in winter acted as a moisture reservoir all year round. The
445 path followed by moist air masses leading to precipitation in the northern Alps were largely dependent on the sea-ice extension in the North Atlantic Ocean. During summer, the North Atlantic was almost ice-free (black dashed lines in Fig. 4; Rhines and Huybers, 2014), representing the source of moisture for central Europe. Conversely, during winter the North Atlantic Sea ice extended towards Europe with a large lobe (Fig. 6; Rhines and Huybers, 2014), reducing the area of moisture reservoir and causing the moist air masses to reach Europe from a southern position. In this framework, the
450 southern Alpine glaciers were fed throughout the year by Mediterranean moisture forced northward by the low-pressure system centered over the Gulf of Genoa (Fig. 6).

In summary, the Genoa low and the relatively warm Mediterranean temperatures were responsible for frequent and intense precipitation events over the southern Alps, while the northern Alpine glaciers were subject to weaker and more sparse precipitation with a predominance of perturbations from the north-west in summer and the west in winter (as driven by the
455 sea ice extent). These circulation patterns can explain the large piedmont glaciers extending in the southern Alpine foreland and the reconstructed envELA gradient across the Alps (Fig. 4).

5 Conclusions

In this work we disentangled the contributions of the atmospheric circulation components and thermodynamic conditions leading to the Alpine glacier advance during the last phase of the LGM using a modeling approach. We highlight that the
460 resolution of our model simulations is among the highest found in paleoclimate studies and this allows us to obtain much higher spatial detail compared to previous work dealing with this issue.

We simulated PI and 21 ka BP climate and atmospheric circulation over the Alps using a multiple nesting approach, based on a chain of three climate model simulations with increasing resolution (MPI-ESM-P Earth system model, 50km resolution regional model RegCM4, and 12 km resolution RegCM4). The high-resolution RegCM4 output data were then used to
465 calculate the environmental Equilibrium Line Altitude (envELA) over the Alpine region, providing new detailed and

physically-based information on the Alpine glaciers at 21 ka BP and at PI coditions. Our reconstruction allows us to better understand the different behaviours of the Alpine glaciers in light of the morphology of their accumulation basins as well as some of the shortcomings between previous LGM glacier reconstructions based on ice-flow dynamics and geomorphological evidence. Our method is based only on simulated temperature and precipitation and is independent of local characteristics of the glacier site (dust, avalanches).

In agreement with available literature, our results show much drier and colder 21 ka BP conditions (−6.6 °C on average) than at PI times over the Alpine region. Differences in precipitation regimes across the Alps were caused by the southward displacement of the North Atlantic storm track, temperature differences controlling convective phenomena, and frequent and persistent occurrence of cyclones and anticyclones. In particular, in the northern Alps, precipitation was sparse and weak, as the Atlantic storm track was located south of the Alps and was subject only to a small seasonal variability caused by the Atlantic sea-ice extension. Conversely, the southern Alpine region received frequent and abundant precipitation due to the interplay of the Genoa low with the relatively warm Mediterranean Sea and convective phenomena. These, in particular, led to summer snowfall at low elevations, preserving the glaciers and lowering the ELA. These results further demonstrate the great potential for the use of RCM-simulated high resolution paleoclimate data in the study of the past cryosphere.

Data availability

The data are available with the DOI: 10.5281/zenodo.7278461.

Author contributions:

Conceptualization: RRC, FG

Methodology: CDG, RRC, FG

Investigation: CDG

Visualization: CDG

Supervision: RRC, FG

Writing—original draft: CDG, RRC, FG

Writing—review & editing: CDG, RRC, GM, MŽ, FG

Competing interests

The authors declare that they have no competing interests.

Acknowledgments

We would like to thank Johann Jungclaus (Max Planck Institute for Meteorology) for providing the MPI-ESM-P simulations, Graziano Giuliani (International Center for Theoretical Physics) for adapting the RegCM4 model to paleoclimate applications and Riccardo Scotti for the comments and corrections.

Funding

CDG has received a doctoral grant from the University of Trieste (Earth Science, Fluid-Dynamics, and Mathematics. Interactions and Methods, Department of Mathematics and Geosciences) and a research fellow grant from the International Center for Theoretical Physics. MŽ has received funding from the Slovenian Research Agency (ARRS) under the programme Dynamic Earth (P1-0419) and the project Past climate change and glaciation at the Alps-Dinarides junction (J1-2479).

References

1. Ahlmann, H.W.S.: Le niveau de glaciation comme fonction de l'accumulation d'humidité sous forme solide: Méthode pour le calcul de l'humidité condensée dans la haute montagne et pour l'étude de la fréquence des glaciers. Geografiska Annaler, 6, 223-272, doi: 10.1080/20014422.1924.11881098, 1924.

2. Amante, C. and Eakins, B.: ETOPO1 1 Arc-Minute Global Relief Model: Procedures, data sources and analysis. NOAA technical memorandum NESDIS NGDC-24, DOI: 10.7289/V5C8276M, 2009.

3. Anderson, R.S., Anderson, L.S., Armstrong, W.H., Rossi, M.W., and Crump, S.E: Glaciation of alpine valleys: The glacier-debris-covered glacier-rock glacier continuum, Geomorphology, 311, 127-142, https://doi.org/10.1016/j.geomorph.2018.03.015, 2018.

4. Annan, J. and Hargreaves, J. C.: A new global reconstruction of temperature changes at the Last Glacial Maximum, Clim. Past, 9, 367-376. https://doi.org/10.5194/cp-9-367-2013, 2013.

5. Auer, I., Böhm, R., Jurkovic, A., Lipa, W., Orlik, A., Potzmann, R., Schöner, W., Ungersböck, M., Matulla, C., Briffa, K., Jones, P., Efthymiadis, D., Brunetti, M., Nanni, T., Maugeri, M., Mercalli, L., Mestre, O., Moisselin, J.-M., Begert, M., Müller-Westermeier, G., Kveton, V., Bochnicek, O., Stastny, P., Lapin, M., Szalai, S., Szentimrey, T., Cegnar, T., Dolinar, M., Gajic-Capka, M., Zaninovic, K., Majstorovic, Z., and Nieplova, E.: HISTALP-historical instrumental climatological surface time series of the Greater Alpine Region, Int. J. Climatol., 27, 17-46, https://doi.org/10.1002/joc.1135, 2007.

6. Bartlein, P.J., Harrison, S.P., Brewer, S., Connor, S., Davis, B.A.S., Gajewski, K., Guiot, J., Harrison-Prentice, T.I., Henderson, A., Peyron, O., Prentice, I.C., Scholze, M., Seppä, H., Shuman, B., Sugita, S., Thompson, R.S., Viau,

A.E., Williams, J., and Wu, H.: Pollen-based continental climate reconstructions at 6 and 21 ka: A global synthesis, Clim. Dynam., 37, 775-802, https://doi.org/10.1007/s00382-010-0904-1, 2010.

7. Becker, P., Seguinot, J., Jouvet, G., and Funk, M.: Last Glacial Maximum precipitation pattern in the Alps inferred from glacier modelling, Geographica Helvetica, 71, 173-187, https://doi.org/10.5194/gh-71-173-2016, 2016.

8. Berger, A.: Long-term variations of caloric insolation resulting from the Earth's orbital elements, Quaternary Res., 9, 139–167, https://doi.org/10.1016/0033-5894(78)90064-9, 1978.

9. Braconnot, P., Harrison, S. P., Kageyama, M., Bartlein, P. J., Masson-Delmotte, V., Abe-Ouchi, A., Otto-Bliesner, B. and Zhao, Y.: Evaluation of climate models using palaeoclimatic data, Nat. Clim. Change, 2, 417-424, https://doi.org/10.1038/NCLIMATE1456, 2012.

10. Clark, P.U., Dyke, A.S., Shakun, J.D., Carlson, A.E., Clark, J., Wohlfarth, B., Mitrovica, J.X., Hostetler, S.W., and McCabe, A.M.: The Last Glacial Maximum, Science, 325, 710-714, https://doi.org/10.1126/science.1172873, 2009.

11. Cogley, J.G., Hock, R., Rasmussen, L.A., Arendt, A.A., Bauder, A., Braithwaite, R.J., Jansson, P., Kaser, G., Möller, M., Nicholson, L. and Zemp, M.: Glossary of Glacier Mass Balance and Related Terms, IHP-VII Technical Documents in Hydrology No. 86, IACS Contribution No. 2, UNESCO-IHP, Paris, 2011.

12. Colucci, R.R.: Geomorphic influence on small glacier response to post-Little Ice Age climate warming: Julian Alps, Europe, Earth Surf. Processes, 41, 1227-1240, https://doi.org/10.1002/esp.3908, 2016.

13. Cossart, E., Fort, M., Bourlès, D., Braucher, R., Perrier, R., and Siame, L.: Deglaciation pattern during the Lateglacial/Holocene transition in the southern French Alps. Chronological data and geographical reconstruction from the Clarée Valley (upper Durance catchment, southeastern France), Palaeogeogr. Paleoecol., 315, 109-123, https://doi.org/10.1016/j.palaeo.2011.11.017, 2012.

14. Danielson, J. J. and Gesch, D. B.: Global multi-resolution terrain elevation data 2010 (GMTED2010). Tech. rep. US Geological Survey. DOI: 10.3133/ofr20111073, 2011.

15. Dee, D.P., Uppala, S.M., Simmons, A.J., Berrisford, P., Poli, P., Kobayashi, S., Andrae, U., Balmaseda, M.A., Balsamo, G., Bauer, D.P., Bechtold, Beljaars, A.C.M., van de Berg, L., Bidlot, J., Bormann, N., Delsol, C., Dragani, R., Fuentes, M., Geer, A.J., Haimberger, L., Healy, S.B., Hersbach, H., Hólm, E.V., Isaksen, L., Kållberg, P., Köhler, M., Matricardi, M., McNally, A.P., Monge-Sanz, B.M., Morcrette, J.-J., Park, B.-K., Peubey, C., de Rosnay, P., Tavolato, C., Thépaut, J.-N., and Vitart, F.: The ERA-Interim reanalysis: Configuration and performance of the data assimilation system, Q. J. Roy. Meteor. Soc., 137, 553-597, https://doi.org/10.1002/qj.828, 2011.

16. Duprat-Oualid, F., Rius, D., Bégeot, C., Magny, M., Millet, L., Wulf, S., and Appelt, O.: Vegetation response to abrupt climate changes in Western Europe from 45 to 14.7 k cal a BP: The Bergsee lacustrine record (Black Forest, Germany), J. Quaternary Sci., 32, 1008-1021, https://doi.org/10.1002/jqs.2972, 2017.

17. Ehlers, J., Gibbard, P.L., and Hughes, P.D. (Eds.): Quaternary Glaciations - Extent and Chronology. A Closer Look, Elsevier Science, London, 2011.

555   18. Elguindi, N., Bi, X., Giorgi, F., Nagarajan, B., Pal, J., Solmon, F., Rauscher, S., Zakey, A., O'Brien, T., Nogherotto, R., and Giuliani, G.: Regional Climate Model RegCM: Reference Manual Version 4.5, Tech. Rep. Abdus Salam ICTP, 2014.

19. Federici, P.R., Ribolini, A., and Spagnolo, M.: Glacial history of the Maritime Alps from the Last Glacial Maximum to the Little Ice Age, Geol. Soc. SP, 433, 137-159, https://doi.org/10.1144/SP433.9, 2017.

560   20. Florineth, D. and Schlüchter, C.: Alpine Evidence for Atmospheric Circulation Patterns in Europe during the Last Glacial Maximum, Quaternary Res. 54, 295-308, https://doi.org/10.1006/qres.2000.2169, 2000.

21. Fontana, A., Mozzi, P., and Marchetti, M.: Alluvial fans and megafans along the southern side of the Alps, Sediment. Geol., 301, 150-171. https://doi.org/10.1016/j.sedgeo.2013.09.003, 2014.

22. Forno, M. G., Gianotti, F., and Gianluca, R.: Significato paleoclimatico dei rapporti tra il glacialismo principale e
565   quello tributario nella bassa Valle della Dora Baltea, Il Quaternario - Italian Journal of Quaternary Sciences, 23, 105-124, 2010.

23. Giorgi, F.: Thirty years of regional climate modeling: Where are we and where are we going next?, J. Geophys. Res-Atmos., 124, 5696-5723, https://doi.org/10.1029/2018JD030094, 2019.

24. Giorgi, F., Coppola, E., Solmon, F., Mariotti, L., Sylla, M., Bi, X., Elguindi, N., Diro, G., Nair, V., Giuliani, G.,
570   Turuncoglu, U., Cozzini, S., Güttler, I., O'Brien, T., Tawfik, A., Shalaby, A., Zakey, A., Steiner, A., Stordal, F., Sloan, L.C., and Brankovic, C.: RegCM4: model description and preliminary tests over multiple CORDEX domains, Clim. Res., 52, 7-29, https://doi.org/10.3354/cr01018, 2012.

25. Haeberli, W., Hoelzle, M., Paul, F., and Zemp, M.: Integrated monitoring of mountain glaciers as key indicators of global climate change: The European Alps, Ann. Glaciol., 46, 150-160,
575   https://doi.org/10.3189/172756407782871512, 2007.

26. Harris, I., Jones, P., Osborn, T., and Lister, D.: Updated high-resolution grids of monthly climatic observations - the CRU TS3.10 Dataset, Int. J. Climatol., 34, 623-642, https://doi.org/10.1002/joc.3711, 2014.

27. Hughes, P.D., Gibbard, P.L., and Ehlers, J.: Timing of glaciation during the last glacial cycle: Evaluating the concept of a global 'Last Glacial Maximum' (LGM), Earth-Sci. Rev., 125, 171-198,
580   https://doi.org/10.1016/j.earscirev.2013.07.003, 2013.

28. Huss, M., Hock, R.: A new model for global glacier change and sea-level rise. Front. Earth Sci., 3, 54, https://doi.org/10.3389/feart .2015.00054, 2015.

29. Imhof, M., Cohen, D., Seguinot, J., Aschwanden, A., Funk, M., & Jouvet, G.: Modelling a paleo valley glacier network using a hybrid model: An assessment with a Stokes ice flow model. Journal of Glaciology, 65, 1000-1010,
585   doi:10.1017/jog.2019.77, 2019.

30. Imhof, M. A.: Combined climate-ice flow modelling of the Alpine ice field during the Last Glacial Maximum, Ph.D, VAW-ETH, https://doi.org/10.3929/ethz-b-000483937, 2021.

31. Isotta, F.A., Frei, C., Weilguni, V., Perčec Tadić, M., Lassègues, P., Rudolf, B., Pavan, V., Cacciamani, C., Antolini, G., Ratto, S.M., Munari, M., Micheletti, S., Bonati, V., Lussana, C., Ronchi, C., Panettieri, E., Marigo, G., Vertačnik, G.: The climate of daily precipitation in the Alps: Development and analysis of a high-resolution grid dataset from pan-Alpine rain-gauge data. Int. J. Climatol. 34, 1657- 1675,https://doi.org/10.1002/joc.3794, 2014.

32. Ivy-Ochs, S., Schäfer, J., Kubik, P.W., Synal, H.A., and Schlüchter, C.: Timing of deglaciation on the northern Alpine foreland (Switzerland), Eclogae Geol. Helv., 97, 47-55, https://doi.org/10.1007/s00015-004-1110-0, 2004.

33. Ivy-Ochs, S., Kerschner, H., Kubik, P.W., and Schlüchter, C.: Glacier response in the European Alps to Heinrich Event 1 cooling: The Gschnitz stadial, J. Quaternary Sci, 21, 115-130, https://doi.org/10.1002/jqs.955, 2006.

34. Ivy-Ochs, S., Monegato, G., and Reitner, J.M.: The Alps: Glacial landforms from the Last Glacial Maximum, in: European Glacial Landscapes: Maximum Extent of Glaciations, edited by: Palacios, D.,Hughes, P.D., García Ruiz, J.M., de Andrés, N., Elsevier, Amsterdam, 449-460, https://doi.org/10.1016/B978-0-12-823498-3.00008-X, 2022.

35. Jost, A, Lunt, D, Kageyama, M, Abe-Ouchi, A, Peyron, O, Valdes, P., and Ramstein, G.: High-resolution simulations of the last glacial maximum climate over Europe: A solution to discrepancies with continental palaeoclimatic reconstructions?, Clim. Dynam., 24, 577-590, https://doi.org/10.1007/s00382-005-0009-4, 2005.

36. Jouvet, G., Seguinot, J., Ivy-Ochs, S., and Funk, M.: Modelling the diversion of erratic boulders by the Valais Glacier during the last glacial maximum, J. Glaciol., 63, 487-498, https://doi.org/10.1017/jog.2017.7, 2017.

37. Kageyama, M., Laîné, A., Abe-Ouchi, A., Braconnot, P., Cortijo, E., Crucifix, M., de Vernal, A., Guiot, J., Hewitt, C.D., and Kitoh, A.: Last Glacial Maximum temperatures over the North Atlantic, Europe and western Siberia: A comparison between PMIP models, MARGO sea–surface temperatures and pollen-based reconstructions, Quaternary Sci. Rev., 25, 2082-2102, https://doi.org/10.1016/j.quascirev.2006.02.010, 2006.

38. Kageyama, M., Harrison, S.P., Kapsch, M.L., Lofverstrom, M., Lora, J.M., Mikolajewicz, U., Sherriff-Tadano, S., Vadsaria, T., Abe-Ouchi, A., Bouttes, N., Chandan, D., Gregoire, L.J., Ivanovic, R.F., Izumi, K., LeGrande, A.N., Lhardy, F., Lohmann, G., Morozova, P.A., Ohgaito, R., Paul, A., Peltier, W.R., Poulsen, C.J., Quiquet, A., Roche, D.M., Shi, X., Tierney, J.E., Valdes, P.J., Volodin, E., Zhu, J.: The PMIP4 Last Glacial Maximum experiments: preliminary results and comparison with the PMIP3 simulations, Clim. Past, 17, 1065-1089, https://doi.org/10.5194/cp-17-1065-2021, 2021.

39. Kamleitner, S., Ivy-Ochs, S., Monegato, G., Gianotti, F., Akçar, N., Vockenhuber, C., Christl, M., and Synal, H.-A.: The Ticino-Toce glacier system (Swiss-Italian Alps) in the framework of the Alpine Last Glacial Maximum, Quaternary Sci. Rev., 279, 107400, https://doi.org/10.1016/j.quascirev.2022.107400, 2022.

40. Kelly, M.A., Buoncristiani, J.F., and Schlchter, C.: A reconstruction of the last glacial maximum (LGM) ice-surface geometry in the western Swiss Alps and contiguous Alpine regions in Italy and France, Eclogae Geol. Helv., 97, 57-75, https://doi.org/10.1007/s00015-004-1109-6, 2004.

41. Kirtman, B., Power, S.B., Adedoyin, A.J., Boer, G.J., Bojariu, R., Camilloni, I., Doblas-Reyes, F., Fiore, A.M., Kimoto, M., Meehl, G., Prather, M., Sarr, A., Schar, C., Sutton, R., van Oldenborgh, G.J., Vecchi, G., and Wang,

H.J.: Near-term climate change: Projections and predictability, in: Climate Change 2013. The Physical Science Basis. Contribution of Working Group I to the Fifth Assessment Report of the Intergovernmental Panel on Climate Change, edited. by: Stocker, T., Qin, D., Plattner, G.K., Tignor, M., Allen, S., Boschung, J., Nauels, A., Xia, Y.,

625   Bex V., and Midgley, P., Cambridge University Press, Cambridge, United Kingdom and New York, NY, USA, https://doi.org/10.1017/CBO9781107415324.023, 2013.

42. Kuhlemann, J., Rohling, E. J., Krumrei, I., Kubik, P., Ivy-Ochs, S., and Kucera, M.: Regional synthesis of Mediterranean atmospheric circulation during the Last Glacial Maximum, Science, 321, 1338-1340, https://doi.org/10.1126/science.1157638, 2008.

630   43. Laîné, A., Kageyama, M., Salas-Mélia, D., Voldoire, A., Riviere, G., Ramstein, G., Planton, S., Tyteca, S., and Peterschmitt, J. Y.: Northern hemisphere storm tracks during the last glacial maximum in the PMIP2 ocean-atmosphere coupled models: energetic study, seasonal cycle, precipitation; Clim. Dynam., 32, 593-614, https://doi.org/10.1007/s00382-008-0391-9, 2009.

44. Lambeck, K., Rouby, H., Purcell, A., Sun, Y., and Sambridge, M.: Sea level and global ice volumes from the Last

635   Glacial Maximum to the Holocene, Proceedings of the National Academy of Sciences, 111, 15296-15303, https://doi.org/10.1073/pnas.1411762111, 2014.

45. Lie, Ø., Dahl, S.O., and Nesje, A.: A theoretical approach to glacier equilibrium-line altitudes using meteorological data and glacier mass-balance records from southern Norway, The Holocene, 13, 365-372, https://doi.org/10.1191/0959683603hl629rp, 2003.

640   46. Lisiecki, L.E. and Stern, J.V.: Regional and global benthic $\delta^{18}O$ stacks for the last glacial cycle, Paleoceanography, 31, 1368–1394, https://doi.org/10.1002/2016pa003002, 2016.

47. Ludwig, P., Schaffernicht, E.J., Shao, Y., and Pinto, J.G.: Regional atmospheric circulation over Europe during the Last Glacial Maximum and its links to precipitation, J. Geophys. Res., 121, 2130-2145, https://doi.org/10.1002/2015JD024444, 2016.

645   48. Ludwig, P., Pinto, J. G., Raible, C. C., and Shao, Y.: Impacts of surface boundary conditions on regional climate model simulations of European climate during the Last Glacial Maximum, Geophys. Res. Lett., 44, 5086-5095, https://doi.org/10.1002/2017GL073622, 2017.

49. Ludwig, P., Gavrilov, M.B., Markovic, S.B., Ujvari, G., and Lehmkuhl, F.: Simulated regional dust cycle in the Carpathian Basin and the Adriatic Sea region during the Last Glacial Maximum, Quatern. Int., 581, 114-127,

650   https://doi.org/10.1016/j.quaint.2020.09.048, 2021.

50. Luetscher, M., Boch, R., Sodemann, H., Spötl, C., Cheng, H., Edwards, R. L., Frisia, S., Hof, F., and Müller, W.: North Atlantic storm track changes during the Last Glacial Maximum recorded by Alpine speleothems, Nat. Commun., 6, 6344, https://doi.org/10.1038/ncomms7344, 2015.

51. Mcgrath, D., Sass, L, O'Neel, S., Arendt, A., and Kienholz, C.: Hypsometric control on glacier mass balance sensitivity in Alaska and northwest Canada, Earth's Future, 5, 324-336, https://doi.org/10.1002/2016EF000479, 2017.

52. Merz, N., Raible, C.C., and Woollings, T.: North Atlantic Eddy-Driven Jet in Interglacial and Glacial Winter Climates, J. Climate, 28, 3977-3997, https://doi.org/10.1175/jcli-d-14-00525.1, 2015.

53. Mix, A.C., Bard, E., and Schneider, R.: Environmental processes of the ice age: Land, oceans, glaciers (EPILOG), Quaternary Sci. Rev., 20, 627-657, https://doi.org/10.1016/S0277-3791(00)00145-1, 2001.

54. Monegato, G.: Local glaciers in the Julian Prealps (NE Italy) during the Last Glacial Maximum, Alpine and Mediterranean Quaternary, 25, 5-14, 2012.

55. Monegato, G., Ravazzi, C., Donegana, M., Pini, R., Calderoni, and G., Wick, L.: Evidence of a two-fold glacial advance during the last glacial maximum in the Tagliamento end moraine system (eastern Alps), Quaternary Res., 68, 284-302, https://doi.org/10.1016/j.yqres.2007.07.002, 2007.

56. Monegato, G., Ravazzi, C., Culiberg, M., Pini, R., Bavec, M., Calderoni, G., Jež, J., and Perego, R.: Sedimentary evolution and persistence of open forests between the south-eastern Alpine fringe and the Northern Dinarides during the Last Glacial Maximum, Palaeogeogr. Palaeoecol. 436, 23-40, https://doi.org/10.1016/j.palaeo.2015.06.025, 2015.

57. Monegato, G., Scardia, G., Hajdas, I., Rizzini, F., and Piccin, A.: The Alpine LGM in the boreal ice-sheets game, Sci. Rep-UK, 7, 2078, https://doi.org/10.1038/s41598-017-02148-7, 2017.

58. Ohmura, A. and Boettcher, M.: Climate on the equilibrium line altitudes of glaciers: Theoretical background behind Ahlmann's P/T diagram, J. Glaciol., 64, 489-505, https://doi.org/10.1017/jog.2018.41, 2018.

59. Peltier, W.R. and Fairbanks, R.G.: Global glacial ice volume and Last Glacial Maximum duration from an extended Barbados sea level record, Quaternary Sci. Rev., 25, 3322-3337, https://doi.org/10.1016/j.quascirev.2006.04.010, 2006.

60. Peresani, M., Monegato, G., Ravazzi, C., Bertola, S., Margaritora, D., Breda, M., Fontana, A., Fontana, F., Janković, I., Karavanić, I., Komšo, D., Mozzi, P., Pini , R., Furlanetto, G., De Amicis, M.G.M., Perhoč, Z., Posth, C., Ronchi, L., Rossato, S., Vukosavljević, N., and Zerboni, A.: Hunter-gatherers across the great Adriatic-Po region during the Last Glacial Maximum: Environmental and cultural dynamics, Quatern. Int., 581, 367-376, https://doi.org/10.1016/j.quaint.2020.10.007, 2021.

61. Pini, R., Furlanetto, G., Vallé, F., Badino, F., Wick, L., Anselmetti, F.S., Bertuletti, P., Fusi, N., Morlock, M.A., Delmonte, B., Harrison, S.P.: Linking North Atlantic and Alpine Last Glacial Maximum climates via a high-resolution pollen-based subarctic forest steppe record, Quaternary Sci. Rev., 15,107759.,https://doi.org/10.1016/j.quascirev.2022.107759 , 2022.

62. Pinto, J. G. and Ludwig, P.: Extratropical cyclone characteristics over the North Atlantic and Western Europe during the Last Glacial Maximum, Clim. Past, 16, 611-626, https://doi.org/10.5194/cp-16-611-2020, 2020.

63. Preusser, F., Graf, H.R., Keller, O., Krayss, E., and Schlüchter, C.: Quaternary glaciation history of northern Switzerland, E&G Quaternary Science Journal, 60, 282-305, https://doi.org/10.3285/eg.60.2-3.06, 2011.

64. Racoviteanu, A.E., Rittger, K., Armstrong, R.: An automated approach for estimating snowline altitudes in the karakoram and eastern himalaya from remote sensing. Front Earth Sci 7:220. https://doi.org/10.3389/feart.2019.00220, 2019.

65. Ramstein, G., Kageyama, M., Guiot, J., Wu, H., Hély, C., Krinner, G., and Brewer, S.: How cold was Europe at the Last Glacial Maximum? A synthesis of the progress achieved since the first PMIP model-data comparison, Clim. Past, 3, 331-339, https://doi.org/10.5194/cp-3-331-2007, 2007.

66. Ravazzi, C., Pini, R., Badino, F., De Amicis, M., Londeix, L., and Reimer, P.J.: The latest LGM culmination of the Garda Glacier (Italian Alps) and the onset of glacial termination. Age of glacial collapse and vegetation chronosequence, Quaternary Sci. Rev., 105, 26-47, https://doi.org/10.1016/j.quascirev.2014.09.014, 2014.

67. Rettig, L., Monegato, G., Mozzi, P., Žebre, M., Casetta, L., Fernetti, M., and Colucci, R.R.: The Pleistocene evolution and reconstruction of LGM and late glacial paleoglaciers of the Silisia Valley and Mount Raut (Carnic Prealps, NE Italy), Alpine and Mediterranean Quaternary, 34, 277-290, 2021.

68. Rhines, A. and Huybers, P.J.: Sea ice and dynamical controls on preindustrial and last glacial maximum accumulation in central Greenland, J. Climate, 27, 8902-8917, https://doi.org/10.1175/JCLI-D-14-00075.1, 2014.

69. Salcher, B.C., Hinsch, R., and Wagreich, M.: High-resolution mapping of glacial landforms in the North Alpine Foreland, Austria., Geomorphology, 122, 283-293, https://doi.org/10.1016/j.geomorph.2009.09.037, 2010.

70. Scapozza, C., Castelletti, C., Soma, L., Dall'Agnolo, S., and Ambrosi, C.: Timing of LGM and deglaciation in the Southern Swiss Alps, Géomorphologie: relief, processus, environnement, 20, 307-322, https://doi.org/10.4000/geomorphologie.10753, 2014.

71. Schaffernicht, E.J., Ludwig, P., and Shao, Y.: Linkage between dust cycle and loess of the Last Glacial Maximum in Europe, Atmos. Chem. Phys., 20, 4969-4986, https://doi.org/10.5194/acp-20-4969-2020, 2020.

72. Schmittner, A., Urban, N. M., Shakun, J. D., Mahowald, N. M., Clark, P. U., Bartlein, P. J., Mix, A.C., Rosell-Melé, A.: Climate sensitivity estimated from temperature reconstructions of the Last Glacial Maximum. *Science*, *334*, 1385-1388, doi:10.1126/science.1203513, 2011.

73. Scotti, R., Brardinoni, F., Crosta, G. B., Cola, G., and Mair, V.: Time constraints for post-LGM landscape response to deglaciation in Val Viola, Central Italian Alps, Quaternary Sci. Rev., 177, 10-33, https://doi.org/10.1016/j.quascirev.2017.10.011, 2017.

74. Seguinot, J., Ivy-Ochs, S., Jouvet, G., Huss, M., Funk, M., and Preusser, F.: Modelling last glacial cycle ice dynamics in the Alps, Cryosphere, 12, 3265-3285, https://doi.org/10.5194/tc-12-3265-2018, 2018.

75. Sirocko, F., Knapp, H., Dreher, F., Förster, M., Albert, J., Brunck, H., Veres, D., Dietrich, S., Zech, M., Hambach, U., Röhner, M., Rudert, S., Schwibus, K., Adams, C., and Sigl, P.: The ELSA-Vegetation-Stack: Reconstruction of

Landscape Evolution Zones (LEZ) from laminated Eifel maar sediments of the last 60,000 years, Global Planet. Change, 142, 108-135, https://doi.org/10.1016/j.gloplacha.2016.03.005, 2016.

76. Snyder, C.: Evolution of global temperature over the past two million years, *Nature,* 538, 226–228, https://doi.org/10.1038/nature19798, 2016.

77. Spötl, C., Koltai, G., Jarosch, A.H., and Cheng, H.: Increased autumn and winter precipitation during the Last Glacial Maximum in the European Alps, Nat. Commun., 12, 1-9, https://doi.org/10.1038/s41467-021-22090-7, 2021.

78. Stadelmaier, K.H., Ludwig, P., Bertran, P., Antoine, P., Shi, X., Lohmann, G., and Pinto, J. G.: A new perspective on permafrost boundaries in France during the Last Glacial Maximum, Clim. Past, 17, 2559-2576, https://doi.org/10.5194/cp-17-2559-2021, 2021.

79. Stevens, B., Giorgetta, M., Esch, M., Mauritsen, T., Crueger, T., Rast, S., Salzmann, M., Schmidt, H., Bader, J., Block, K., Brokopf, R., Fast, I., Kinne, S., Kornblueh, L., Lohmann, U., Pincus, R., Reichler, and T., Roeckner, E.: Atmospheric component of the MPI-M Earth system model: ECHAM6, J. Adv. Model. Earth Sy., 5, 146-172, https://doi.org/10.1002/jame.20015, 2013.

80. Strandberg, G., Brandefelt, J., Kjellstro, E., and Smith, M.B.: High-resolutionregional simulation of last glacial maximum climate in Europe, Tellus A: Dynamic Meteorology and Oceanography, 63, 107-125, https://doi.org/10.1111/j.1600-0870.2010.00485.x, 2011.

81. Tierney, J.E., Zhu, J., King, J., King, J., Malevich, S.B., Hakim, G.J.,Poulsen, C.J.: Glacial cooling and climate sensitivity revisited, Nature 584, 569–573, https://doi.org/10.1038/s41586-020-2617-x, 2020.

82. Tzedakis, P.C.: Towards an understanding of the response of southern European vegetation to orbital and suborbital climate variability, Quaternary Sci. Rev., 24, 1585-1599, https://doi.org/10.1016/j.quascirev.2004.11.012, 2005.

83. Velasquez, P., Messmer, M., and Raible, C. C.: A new bias-correction method for precipitation over complex terrain suitable for different climate states: a case study using WRF (version 3.8.1), Geosci. Model Dev., 13, 5007–5027, https://doi.org/10.5194/gmd-13-5007-2020, 2020.

84. Velasquez, P., Kaplan, J. O., Messmer, M., Ludwig, P., and Raible, C. C.: The role of land cover in the climate of glacial Europe, Clim. Past, 17, 1161–1180, https://doi.org/10.5194/cp-17-1161-2021, 2021.

85. Velasquez, P., Messmer, M., and Raible, C. C.: The role of ice-sheet topography in the Alpine hydro-climate at glacial times, Clim. Past, 18, 1579–1600, https://doi.org/10.5194/cp-18-1579-2022, 2022.

86. Višnjević, V., Herman, F., and Prasicek, G.: Climatic patterns over the European Alps during the LGM derived from inversion of the paleo-ice extent, Earth Planet. Sc. Lett., 538, 116185, https://doi.org/10.1016/j.epsl.2020.116185, 2020.

87. Watts, W., Allen, J., and Huntley, B: Vegetation history and palaeoclimate of the last glacial period at Lago Grande di Monticchio, southern Italy, Quaternary Sci. Rev. 15, 133-153, https://doi.org/10.1016/0277-3791(95)00093-3, 1996.

755   88. Wirsig, C., Zasadni, J., Christl, M., Akçar, N., and Ivy-Ochs, S.: Dating the onset of LGM ice surface lowering in the High Alps. Quaternary Sci. Rev., 143, 37-50, https://doi.org/10.1016/j.quascirev.2016.05.001, 2016.

89. Wu, H., Guiot, J., Brewer, S., and Guo, Z.: Climatic changes in Eurasia and Africa at the last glacial maximum and mid-Holocene: reconstruction from pollendata using inverse vegetation modelling, Clim. Dynam., 29, 211-229, https://doi.org/10.1007/s00382-007-0231-3, 2007.

760   90. Yokoyama, Y., Lambeck, K., De Deckker, P., Johnston, P., and Fifield, L.K.: Timing of the Last Glacial Maximum from observed sea-level minima, Nature, 406, 713-716, https://doi.org/10.1038/35021035, 2000.

91. Žebre, M., Colucci, R.R., Giorgi, F., Glasser, N.F., Racoviteanu, A.E., and Del Gobbo, C.: 200 years of equilibrium-line altitude variability across the European Alps (1901-2100), Clim. Dynam., 56, 1183-1201, https://doi.org/10.1007/s00382-020-05525-7, 2021.

765   92. Zekollari, H., Huss, M., Farinotti, D.: On the Imbalance and Response Time of Glaciers in the European Alps, Geophys. Res. Lett. 47, e2019GL085578. https ://doi.org/10.1029/2019G L0855 78, 2020.

93. Zemp, M., Paul, F., Hoelzle, M., and Haeberli, W.: Glacier fluctuations in the European Alps, in: Darkening Peaks: Glacier Retreat, edited by: Orlove, B., Wiegandt, E., Luckman, and B.H., Berkeley, US, 152–167, 2008.